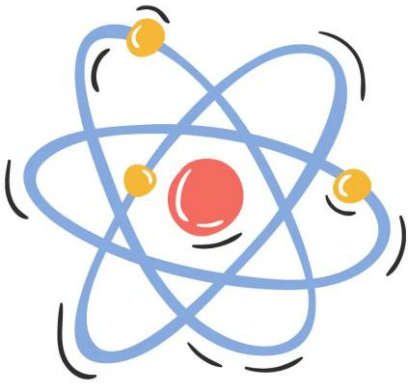

ISSN: 1672 - 6553

JOURNAL OF DYNAMICS AND CONTROL

VOLUME 10 ISSUE 01: P153 - 176

ANALYSIS OF THREE-DIMENSIONAL CASSON FLUID FLOW AND HEAT TRANSFER INFLUENCED BY HOMOGENEOUS AND HETEROGENEOUS REACTION MECHANISMS

S. Kemparaju[1], R. D. Jagadeesha[2], M. S. Sunitha[3], *P. B. Sampath Kumar*[4,5]

[1] Department of Mathematics, Government First Grade College, Ramanagara, Karnataka, India

[2] Department of Mathematics, Government First Grade College for Women, Holenarasipura, Karnataka, India

[3] Department of Mathematics, Government First Grade College, Tumkur, Karnataka, India

[4] Department of Studies and Research in Mathematics, Ramanagara PG Centre, Bangalore University, Karnataka 562159, India

[5] Universidad Bernardo O'Higgins, Facultad de Ingeniería, Ciencia y Tecnología, Departamento de Formación y Desarrollo Científico en Ingeniería, Av. Viel 1497, Santiago, Chile

JOURNAL OF DYNAMICS AND CONTROL
https://doi.org/10.71058/jodac.v10i01009

ANALYSIS OF THREE-DIMENSIONAL CASSON FLUID FLOW AND HEAT TRANSFER INFLUENCED BY HOMOGENEOUS AND HETEROGENEOUS REACTION MECHANISMS

S. Kemparaju[1], R. D. Jagadeesha[2], M. S. Sunitha[3], *P. B. Sampath Kumar[4],[5]*

[1] *Department of Mathematics, Government First Grade College, Ramanagara, Karnataka, India*
[2] *Department of Mathematics, Government First Grade College for Women, Holenarasipura, Karnataka, India*
[3] *Department of Mathematics, Government First Grade College, Tumkur, Karnataka, India*
[4] *Department of Studies and Research in Mathematics, Ramanagara PG Centre, Bangalore University, Karnataka 562159, India*
[5] *Universidad Bernardo O'Higgins, Facultad de Ingeniería, Ciencia y Tecnología, Departamento de Formación y Desarrollo Científico en Ingeniería, Av. Viel 1497, Santiago, Chile*
skemparaju74@gmail.com, jagadeesh25docs@gmail.com, ms.sunitha0204@gmail.com, sampathkumarpb123@gmail.com
[*]***Corresponding Author: S. Kemparaju***

Abstract: The present study examines the magnetohydrodynamic flow of a Casson fluid over a stretching sheet while accounting for homogeneous and heterogeneous chemical reactions. The model further incorporates Joule heating, viscous dissipation, nonlinear thermal convection, and radiative heat transfer relevant to moderately high temperatures. The resulting system of nonlinear ordinary differential equations is tackled numerically using the RKF-45 method combined with a shooting technique. The influence of key physical parameters on the velocity, temperature, and concentration fields is thoroughly analyzed through graphical and tabulated results. The findings indicate that increases in homogeneous and heterogeneous reaction parameters reduce species concentration and shrink the associated boundary layers, while stronger thermal radiation and higher temperature-ratio parameters elevate the fluid temperature.

Keywords: Casson fluid, homogeneous, heterogeneous, viscous dissipation, radiation.

Introduction

Casson fluid is a non-Newtonian model characterized by yield stress, where the material behaves like a solid until the applied shear stress exceeds a critical value. Once this threshold is crossed, the viscosity decreases with increasing shear rate, making the Casson model effective for representing many industrial and biological fluids, including blood, chocolate, inks, and polymer solutions. Owing to its ability to capture both shear-thinning and yield-stress

https://doi.org/10.71058/jodac.v10i01009

behaviour, it has become an important model in fluid mechanics and heat transfer studies. With growing applications in biomedical systems, polymer processing, coating technologies, lubrication, and thermal management, research on Casson fluid flows has expanded rapidly. Because of these applications, the Casson fluid model has been extensively investigated for boundary-layer flows under various physical conditions. The classical formulation proposed by Casson [1] established its relevance to yield-stress fluids, particularly pigment-oil suspensions. Building on this foundation, numerous studies have applied the Casson model to engineering and industrial flow systems. Mustafa et al. [2] analysed stagnation-point flow and heat transfer of Casson fluid and reported that the yield stress reduces velocity gradients in the boundary layer. Nadeem and Lee [3] further explored magnetohydrodynamic (MHD) Casson flow over stretching surfaces, showing that magnetic fields enhance flow resistance and thicken the thermal boundary layer. Slip effects on Casson flows have been addressed by Bhattacharyya [4], who demonstrated that velocity slip significantly alters surface shear stress. Chemical reaction effects were examined by Makanda et al. [5], revealing that reaction kinetics strongly modify concentration distributions. Studies by Hayat et al. [6] have highlighted the influence of thermal radiation and internal heat generation on Casson fluid behaviour, demonstrating their significant impact on heat transfer rates. Research on Casson nanofluids also indicates that nanoparticle volume fraction and Brownian motion play critical roles in controlling temperature and concentration fields (Khan & Pop [7]; Nadeem et al., [8]).

In recent years, considerable attention has been directed toward non-Newtonian fluids involving homogeneous-heterogeneous reactions due to their wide relevance in industrial and natural processes. Such reactions frequently arise in food processing, atmospheric and environmental flows, biochemical systems, polymer fabrication, and ceramic manufacturing. The combined effects of heat and mass transfer with coupled homogeneous–heterogeneous reactions are particularly important in applications such as drying technologies, agricultural temperature regulation, fog formation, crop protection, and energy transfer in cooling towers. Chambre and Acrivos [9] conducted one of the earliest analyses of isothermal catalytic reactions in a laminar boundary-layer flow and determined the surface concentration without imposing restrictive assumptions on the reaction mechanism. Later, Chaudhary and Merkin ([10],[11]) developed a simplified isothermal model for coupled homogeneous-heterogeneous reactions in boundary-layer flow, considering both equal and unequal diffusivities of the reactant and auto-catalyst. Further advancements include the work of Khan and Pop [12], who examined stagnation-point flow toward a permeable surface with coupled reactions. The

https://doi.org/10.71058/jodac.v10i01009

influence of homogeneous-heterogeneous reactions on stretching sheet flows was also explored by Kameswaran et al. [13]. Hayat et al. [14] investigated mass transfer in viscoelastic fluid flow over a stretching cylinder in the presence of homogeneous–heterogeneous reactions. Nai-Li Xu et al. [15] investigated homogeneous–heterogeneous reactions in nanofluid flow using Buongiorno's model, where first-order homogeneous reactions occur in the fluid and cubic autocatalytic heterogeneous reactions take place on the wall. Through stagnation-point flow analysis, the study demonstrated multiple solution branches driven by hysteresis-type bifurcations under varying physical parameters. Nisar et al. [16] investigated the homogeneous-heterogeneous reactions on Darcy-Forchheimer nanofluid flow system. Ramya et al. [17] analysed micropolar nanofluid flow over an exponentially stretching surface with homogeneous–heterogeneous reactions using the Cattaneo–Christov heat flux model, highlighting the roles of thermophoresis, Brownian motion, and micropolar effects. The dimensionless governing equations were solved numerically with bvp4c to evaluate the resulting heat and mass transfer behaviour.

The study of natural, forced, and mixed convection flows has gained significant attention due to its wide engineering applications, including nuclear reactor cooling, solar energy collection, thermal storage, electronic cooling, food processing, and cryogenic systems. Within this context, Gorla and Sidawi [16] analyzed free convection over a stretching elastic plate with transpiration cooling, while Wang [17] examined mixed convection heat transfer of non-Newtonian fluids along vertical surfaces. Chamkha [18] studied hydromagnetic natural convection on a linearly stretching plate, and Rashidi et al. [19] provided analytical solutions for mixed convection boundary-layer flow of micropolar fluids using the homotopy analysis method. Giressha et al. [20] further explored mixed convection in a particle-laden Maxwell fluid with nonlinear radiation and variable heat sources. Although extensive literature exists on convection flows under various configurations [21–24], most studies rely on linear thermal convection, which assumes small temperature differences between the surface and surrounding fluid. However, in practical systems—such as solar collectors, electronic cooling devices, nuclear reactors, and thermal energy storage units—buoyancy forces often exhibit nonlinear dependence on temperature, significantly affecting flow and heat transfer. Motivated by this, several researchers, including Vajravelu et al. [25], Kameswaran et al. [26], and Sachin et al. [27], have investigated nonlinear convection effects. More recent contributions include the work of Jyoti et al. [28], who analyzed nonlinear convection with radiative heat transfer in kerosene–alumina nanofluid between parallel plates, and Magammad et al. [29], who studied

https://doi.org/10.71058/jodac.v10i01009

buoyancy-driven nonlinear combined convection with thermal radiation over a nonlinearly stretching vertical sheet.

Despite extensive research on Casson fluids, MHD flows, and convection–radiation effects, only limited studies have addressed the combined influence of nonlinear thermal convection, viscous dissipation, Joule heating, and radiative heat transfer in the presence of simultaneous homogeneous-heterogeneous reactions. Most existing works either neglect yield-stress behavior, consider only linear convection, or omit reaction kinetics from the thermal-mass transport analysis. Furthermore, the interaction between magnetic fields, chemical reactions, and heat generation mechanisms in Casson fluid flow over stretching surfaces remains insufficiently explored. To bridge these gaps, the present study investigates the magnetohydrodynamic flow of a Casson fluid over a stretching sheet by incorporating homogeneous–heterogeneous reactions alongside Joule heating, viscous dissipation, nonlinear convection, and nonlinear radiation. The governing nonlinear ODE system is solved numerically using the RKF-45 method with a shooting scheme, providing new insights into the coupled transport phenomena of Casson fluids under complex thermal and chemical conditions.

Mathematical formulation

The study investigates the three-dimensional nonlinear flow of Casson fluid over a stretching sheet. Homogeneous and heterogeneous reaction mechanisms are incorporated to enhance the mass-transfer characteristics. A Cartesian coordinate system (x, y, z) is employed with the origin fixed at point O, and the motion of the fluid is assumed to occur predominantly along the z-axis. The sheet stretches in the x- and y-directions with velocities $U_w = ax$ and $V_w = ay$, respectively, where $a$and b represent stretching constants. A uniform magnetic field B_0 is imposed in the z-direction, as illustrated in figure 1. The surface temperature is held constant at T_w, while T_∞ represents the ambient temperature outside the thermal boundary layer.

https://doi.org/10.71058/jodac.v10i01009

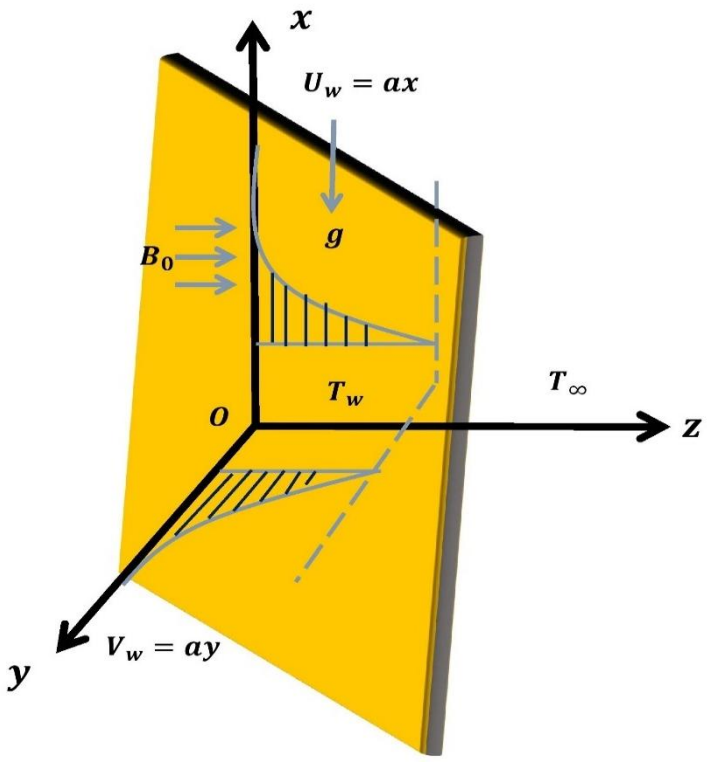

Figure 1: Diagram depicting the physical setup of the flow problem.

For an isotropic Casson fluid, the corresponding rheological model is defined:

$$\tau^{1/n} = \tau_0^{1/n} + \mu\dot{\gamma}^{1/n},$$

$$\begin{cases} 2\left(\mu_B + \frac{P_y}{\sqrt{2\pi}}\right) e_{ij}\ \pi > \pi_c \\ 2\left(\mu_B + \frac{P_y}{\sqrt{2\pi}}\right) e_{ij}\ \pi < \pi_c \end{cases}$$

In the above expression, $\pi = e_{ij}e_{ij}$, where e_{ij}denotes the $(i,j)^{\text{th}}$component of the deformation-rate tensor. The term πrepresents the inner product of the deformation-rate components, while $\pi_c$signifies its critical value associated with the non-Newtonian characteristics of the fluid. Here, $\pi_B$denotes the plastic dynamic viscosity, and $P_y$corresponds to the yield stress. Although several studies consider the flow index as $n = 1$, many practical situations involve $n > 1$.

The preceding assumptions yield the following expressions:

$$\frac{\partial \bar{U}}{\partial x} + \frac{\partial \bar{V}}{\partial y} + \frac{\partial \bar{W}}{\partial z} = 0, \tag{1}$$

$$u\frac{\partial \bar{U}}{\partial x} + v\frac{\partial \bar{U}}{\partial y} + w\frac{\partial \bar{U}}{\partial z} = \nu\left(\left(1 + \frac{1}{\beta}\right)\frac{\partial^2 \bar{U}}{\partial z^2}\right) - \frac{\sigma B_0^2}{\rho}\bar{U}$$

$$+ g\{\beta_0(T - T_\infty) + \beta_1(T - T_\infty)^2\}, \tag{2}$$

https://doi.org/10.71058/jodac.v10i01009

$$u\frac{\partial \bar{V}}{\partial x}+v\frac{\partial \bar{V}}{\partial y}+w\frac{\partial \bar{V}}{\partial z}=\nu\left(\left(1+\frac{1}{\beta}\right)\frac{\partial^2 \bar{U}}{\partial z^2}\right)-\frac{\sigma B_0^2}{\rho}\bar{V}, \tag{3}$$

$$\bar{U}\frac{\partial T}{\partial x}+\bar{V}\frac{\partial T}{\partial y}+\bar{W}\frac{\partial T}{\partial z}=\alpha_m\left(\frac{\partial^2 T}{\partial z^2}\right)-\frac{1}{\rho c_p}\frac{\partial q_r}{\partial z}+\frac{\mu}{\rho c_p}\left(1+\frac{1}{\beta}\right)\left[\left(\frac{\partial \bar{U}}{\partial z}\right)^2+\left(\frac{\partial \bar{V}}{\partial z}\right)^2\right]$$

$$+\frac{\sigma B_0^2}{\rho c_p}\left[\bar{U}^2+v^2\right], \tag{4}$$

$$\bar{U}\frac{\partial a_1}{\partial x}+\bar{V}\frac{\partial a_1}{\partial y}+\bar{W}\frac{\partial a_1}{\partial z}=D_A\frac{\partial^2 a_1}{\partial z^2}-k_c a_1 b_1^2 \tag{5}$$

$$\bar{U}\frac{\partial b_1}{\partial x}+\bar{V}\frac{\partial b_1}{\partial y}+\bar{W}\frac{\partial b_1}{\partial z}=D_B\frac{\partial^2 b_1}{\partial z^2}+k_c a_1 b_1^2 \tag{6}$$

In which $\bar{U},\bar{V}$ and $\bar{W}$ are the velocity components in x, y and z directions respectively, ν the kinematic viscosity coefficient, β the Casson fluid parameter, Γ the time constant, ρ the density of the fluid, σ the electric conductivity, B_0 the magnetic field, g the acceleration due to gravity, β_0 and β_1 the linear and non-linear volumetric thermal expansion coefficient, T the temperature, D_A and D_B the respective diffusion coefficients, a_1, b_1 the concentrations of the chemical species, k_c and k_s the rate constants and we assume that both the chemical reactions are isothermal. It is worth to mention that the Newtonian fluid model can be recover for $\beta \to \infty$ and $n = 1$.

The radiative heat flux expression in equation (4) is given by;

$$q_r=-\frac{4\sigma^*}{3k^*}\frac{\partial T^4}{\partial z}=-\frac{16\sigma^*}{3k^*}T^3\frac{\partial T}{\partial z}, \tag{7}$$

where σ^* and k^* are the Stefan-Boltzman constant and the mean absorption coefficient respectively, and in view to equation (7) in Eq. (4) reduces to;

$$u\frac{\partial T}{\partial x}+v\frac{\partial T}{\partial y}+w\frac{\partial T}{\partial z}=\alpha_m\left(\frac{\partial^2 T}{\partial z^2}\right)+\frac{16\sigma^*}{3\rho c_p k^*}\left[T^3\frac{\partial^2 T}{\partial z^2}+3T^2\left(\frac{\partial T}{\partial z}\right)^2\right]$$

$$+\frac{\mu}{\rho c_p}\left(1+\frac{1}{\beta}\right)\left[\left(\frac{\partial \bar{U}}{\partial z}\right)^2+\left(\frac{\partial \bar{V}}{\partial z}\right)^2\right]+\frac{\sigma B_0^2}{\rho c_p}\left[\bar{U}^2+\bar{V}^2\right], \tag{8}$$

The corresponding boundary conditions are given by;

$$\bar{U}=U_w(x)=ax,\quad \bar{V}=V_w(x)=ay,\quad \bar{W}=0,\quad T=T_w,$$

$$D_A\frac{\partial a_1}{\partial z}=k_s a_1,\quad D_B\frac{\partial b_1}{\partial z}=-k_s a_1 \quad \text{at} \quad z=0,$$

$$\bar{U}\to 0,\quad \bar{V}\to 0,\quad T\to T_\infty,\quad a_1\to a_0,\quad b_1\to 0 \quad \text{as} \quad z\to\infty, \tag{9}$$

https://doi.org/10.71058/jodac.v10i01009

here $U_w = ax$ and $V_w = ay$ are the stretching velocities, a_0 is positive constant.

Now introduce stretching transformations

$$\bar{U} = bxf'(\eta),\ \ \bar{V} = byg'(\eta)$$

$$\bar{W} = -\sqrt{b\nu}\big(F(\eta) + G(\eta)\big),\ \ \eta = z\sqrt{\frac{b}{\nu}},$$

$$T = T_\infty(1 + (\theta_w - 1)\theta(\eta)),\ \theta_w = \frac{T_w}{T_\infty}$$

$$\phi(\eta) = \frac{a_1}{a_0}, H(\eta) = \frac{b_1}{a_0}. \tag{10}$$

in to Eqns. (2) to (6). One can we have;

$$\left(1 + \frac{1}{\beta}\right)F''' + (F + G)F'' - F'^2 - MF' + \lambda(\theta + \alpha\theta^2) = 0, \tag{11}$$

$$\left(1 + \frac{1}{\beta}\right)G''' + (F + G)G'' - G'^2 - MG' = 0, \tag{12}$$

$$\theta'' + R[(1 + (\theta_w - 1)\theta)^3\theta'' + 3(\theta_w - 1)\theta'^2(1 + (\theta_w - 1)\theta)^2] + \Pr(F + G)\,\theta'$$

$$+\left(1 + \frac{1}{\beta}\right)\frac{PrEc_x}{\lambda^2}F''^2 + \left(1 + \frac{1}{\beta}\right)\frac{PrEc_y}{C_1^2}G''^2 + \frac{PrM}{C_1^2}\left[Ec_xF'^2 + Ec_yG'^2\right] = 0, \tag{13}$$

$$\frac{1}{Sc}\phi'' + (F + G)\phi' - K\phi H^2 = 0, \tag{14}$$

$$\frac{\delta}{Sc}H'' + (F + G)H' + K\phi H^2 = 0 \tag{15}$$

The transformed boundary conditions are as follows;

$$F(\eta) = 0, G(\eta) = 0, F'(\eta) = C_1, G'(\eta) = C_1, \theta(\eta) = 1,$$

$$\phi'(\eta) = K_s\phi(\eta), \delta H'(\eta) = -K_s\phi(\eta) \text{ at } \eta = 0,$$

$$F'(\eta) \to 0, G'(\eta) \to 0, \theta(\eta) \to 0, \phi(\eta) \to 1, H(\eta) \to 0 \text{ as } \eta \to \infty, \tag{16}$$

here $M = \frac{\sigma B_0^2}{\rho b}$ -magnetic parameter, $C_1 = \frac{a}{b}$ -stretching ratio parameter, $\lambda = \frac{Gr_x}{Re_x^2}$ -mixed convection parameter, $\alpha = \frac{\beta_1}{\beta_0}(T_w - T_\infty)$ -nonlinear convection parameter, $Gr_x = \frac{g\beta_0(T_w - T_\infty)U_w^3}{\nu^2 a^3}$ -Grashof number, $Pr = \frac{\nu}{\alpha_m}$ -Prandtl number, $R = \frac{16\sigma^* T_\infty^3}{3k^* k}$ - thermal radiation parameter, $\theta_w = \frac{T_w}{T_\infty}$ - temperature ratio parameter, $Ec_x = \frac{U_w^2}{c_p(T_w - T_\infty)}$ -Eckert number along x

https://doi.org/10.71058/jodac.v10i01009

direction, $Ec_y = \frac{V_w^2}{c_p(T_w - T_\infty)}$ -Eckert number along y direction, $Sc = \frac{\nu}{D_A}$ -Schmidt number, $\delta = \frac{D_B}{D_A}$ -ratio of diffusion coefficient, $K = \frac{k_c a_0^2}{b}$ -strength of the homogeneous reaction parameter, $K_S = \frac{k_s}{D_A}\sqrt{\frac{\nu}{b}}$-strength of the heterogeneous-reaction parameter, $Re_x = \frac{U_w^2}{\nu a}$ local Reynolds number.

For the most of real time practical applications we assume that chemical diffusion coefficients are almost same size. So diffusion coefficients are equal i.e. $\delta = 1$

$$\phi(\eta) + H(\eta) = 1 \tag{18}$$

Then by substituting equation (18) in (14) and (15), we get

$$\frac{1}{Sc}\phi'' + (F + G)\phi' - K\phi(1 - \phi)^2 = 0, \tag{19}$$

Subject to the boundary conditions:

$$\phi'(0) = K_s\phi(0), \quad \phi(\infty) = 1 \tag{20}$$

The quantities of practical interest are given by:

$$C_{fx}Re_x^{\frac{1}{2}} = \left[\left(1 + \frac{1}{\beta}\right)F''(0)\right],$$

$$C_{fy}Re_x^{\frac{1}{2}} = \left[\left(1 + \frac{1}{\beta}\right)G''(0)\right],$$

$$Re_x^{-\frac{1}{2}}Nu_x = -(1 + R\theta_w^3)\theta'(0),$$

$$Re_x^{-\frac{1}{2}}Sh_x = -\phi'(0), \tag{21}$$

Method of Solution

The obtained system of non-linear Ode's is of third order in F & G and of second order in θ & ϕ with inter-related boundary conditions. To solve such complicated system numerically; we apply Runge-Kutta method based on shooting technique. The technique generally transformed boundary valued problem into initial value problem and based on the step size for the precise solution of problem.

https://doi.org/10.71058/jodac.v10i01009

Physical Insight into the Results

The numerical simulations are performed by considering combined variations of the magnetic parameter M, stretching ratio C_1, mixed convection parameter λ, nonlinear convection parameter α, thermal radiation parameter R, temperature ratio θ_w, Eckert numbers along the x- and y-directions (Ec_x, Ec_y), Schmidt number Sc, and the homogeneous and heterogeneous reaction strengths K and K_s. Their influences on the velocity, temperature, and concentration distributions are illustrated through graphical results, whereas the skin-friction coefficients and the local Nusselt and Sherwood numbers are presented in tabulated form (see Tables 1 and 2). For the parametric study, each profile is plotted by varying only one parameter at a time while keeping the others fixed at $E_{cx} = E_{cy} = 0.05, K = K_s = 1, M = 2, Pr = 6.2, \theta_w = 2, Sc = 0.6, \lambda = C_1 = \alpha = 0.5$, and $R = 0.5$. Tables 1 and 2 present the computed values of the skin-friction coefficients, along with the local Nusselt and Sherwood numbers, for the selected parameters of the Casson fluid model. The results show that the axial and transverse skin-friction coefficients $(C_{fx}Re_x^{0.5}, C_{fy}Re_x^{0.5})$ decrease as the magnetic parameter $M$and stretching ratio C_1increase. In contrast, the parameters λ, α, R, θ_w, Ec_x, and Ec_ylead to an increase in the drag force along both directions. The heat-transfer rate (local Nusselt number) rises with increasing C_1, λ, α, R, and θ_w, whereas stronger magnetic effects and higher Eckert numbers (M, Ec_x, Ec_y) suppress thermal transport. The mass-transfer rate (local Sherwood number) is enhanced for higher values of K, while opposite trends are observed for K_s, C_1, λ, α, R, θ_w, Ec_x, and Ec_y.

Figure 2 illustrates the influence of the radiation parameter R on the temperature distribution $\theta(\eta)$. The temperature curves rise noticeably with increasing R, as stronger thermal radiation supplies additional energy to the fluid, thereby elevating the thermal field. This demonstrates that radiation plays a significant role in enhancing the temperature profile. A similar trend is observed for the temperature ratio parameter $\theta_w = T_f/T_w$, as shown in Figure 3. An increase in θ_w results in a thicker thermal boundary layer for the Casson fluid. This behavior occurs because a larger temperature ratio corresponds to a higher surface temperature T_f, which intensifies heat transfer from the sheet to the surrounding fluid. The influence of the Prandtl number Pr on the temperature field $\theta(\eta)$ is shown in 4. It is observed that, an essential aspect of heat-transfer behaviour in non-Newtonian fluids such as the Casson model. An increase in Pr results in a noticeable decline in the temperature distribution throughout the boundary layer. This occurs because the Prandtl number represents the ratio of momentum

https://doi.org/10.71058/jodac.v10i01009

diffusivity to thermal diffusivity. Fluids with higher Pr possess lower thermal diffusivity, meaning that heat is less able to diffuse away from the surface into the surrounding fluid. As Pr increases, the fluid's ability to conduct heat diminishes, which suppresses thermal diffusion and narrows the thermal boundary layer.

Figures 5 and 6 illustrate the influence of the magnetic parameter M on the velocity components. A reduction in both axial and transverse velocities is observed as M increases. This decline occurs because the applied magnetic field introduces a Lorentz force, which acts as a resistive force opposing the motion of the electrically conducting Casson fluid along both the x- and y-directions. Figure 7- 8 are drawn to discuss the effect of stretching ratio parameter C_1 on velocity profiles and temperature profile. It is noticed that, the liquid velocity increase and temperature decrease in case of improved values of $C_1 (= a/b)$. Such effects may also arise because the sheet is stretched in two directions with velocity $U_w = ax$ and $V_w = ay$. The C_1 increase then velocity coefficient a is also increase and creates extra pressure on the sheet due to which rise in liquid flow and drop down the liquid temperature.

The influence of the Schmidt number Sc on the concentration distribution $\phi(\eta)$ for the Casson fluid is shown in figure 9. An increase in $Sc = \nu/D_A$ leads to a reduction in the concentration profile. This behaviour is expected because Sc is inversely related to the Brownian diffusion coefficient D_A. Higher Schmidt numbers correspond to weaker mass diffusivity, meaning the random motion of fluid particles decreases, which in turn suppresses concentration levels within the boundary layer. Figures 10 and 11 depict the effects of the homogeneous reaction parameter $K$and the heterogeneous reaction parameter K_s on $\phi(\eta)$ for the Casson fluid. In both cases, an increase in K or K_s results in a noticeable decline in the concentration profile and a thinning of the associated concentration boundary layer. This reduction occurs because stronger reaction rates intensify the consumption of the diffusing species, thereby lowering concentration distribution throughout the flow domain. The behaviour of $\theta(\eta)$ for different values of Eckert numbers along x and y directions are demonstrated in figures 12 and 13 respectively. Greater values of Eckert numbers (Ec_x, Ec_y) increase the temperature field with related boundary thickness. Mechanism behind that, the larger Eckert number produces additional heat in the liquid due to frictional heating as a result an improvement is observed in $\theta(\eta)$. Figures 14 and 15 illustrate the variations in velocity and temperature profiles for different values of the mixed convection parameter λ. An increase in λ enhances the buoyancy force near the surface, which accelerates the fluid and thickens the velocity boundary layer. The strengthened buoyancy-induced force promotes fluid motion,

https://doi.org/10.71058/jodac.v10i01009

resulting in higher velocities. Consequently, the enhanced convection improves heat transport away from the surface, leading to a reduction in the temperature field.

Conclusions

The numerical analysis reveals that the Casson fluid flow and transport characteristics are significantly influenced by magnetic effects, stretching intensity, mixed convection, radiation, chemical reactions, and thermal parameters. The skin-friction coefficients decrease with increasing magnetic parameter $M$and stretching ratio C_1, while parameters such as λ, α, R, θ_w, Ec_x, and Ec_yenhance surface drag. Heat transfer is strengthened by larger values of C_1, λ, α, R, and θ_w, whereas stronger magnetic fields and higher Eckert numbers suppress it. The local Sherwood number increases with the homogeneous reaction parameter $K$and decreases with K_s, C_1, λ, α, R, θ_w, Ec_x, and Ec_y. Thermal radiation, elevated temperature ratio, and Eckert numbers intensify the temperature field, while higher Prandtl number reduces it by weakening thermal diffusivity. The magnetic parameter diminishes the velocity components due to the Lorentz force, whereas the stretching ratio promotes flow acceleration and reduces the temperature field. Concentration levels decline with increasing Schmidt number and reaction parameters due to reduced diffusivity and species consumption. Finally, intensifying the mixed convection parameter λenhances buoyancy-driven flow, increases velocity, and lowers the temperature field through stronger convective transport. It is worth to mention that the Newtonian fluid model can be recover for $\beta \to \infty$.

Tables and Graphs

Table 1: Numerical values of $C_{fx}Re_x^{0.5}$ and $C_{fy}Re_x^{0.5}$ for various physical parameters.

M	K	K_s	C_1	λ	α	R	θ_w	Ec_x	Ec_y	$C_{fx}Re_x^{0.5}$	$C_{fy}Re_x^{0.5}$
2	1	1	0.5	0.5	0.5	2	2	0.2	0.2	-1.42006	-2.00830
0										-0.43530	-1.04759
1										-0.99005	-1.59532
2										-1.42006	-2.00830

https://doi.org/10.71058/jodac.v10i01009

	0									-1.42006	-2.00830
	0.5									-1.42006	-2.00830
	1									-1.42006	-2.00830
		0								-1.42006	-2.00830
		1								-1.42006	-2.00830
		1.5								-1.42006	-2.00830
			0.5							-1.42006	-2.00830
			1							-4.00608	-4.49161
			2							-10.2063	-10.6503
				0.5						-1.42006	-2.00830
				1						-0.85742	-2.01400
				2						0.23041	-2.02465
					0.5					-1.42006	-2.00830
					1					-1.26143	-2.00970
					2					-0.94767	-2.01244
						0				-1.75425	-2.00360
						1				-1.53271	-2.00628
						2				-1.42006	-2.00830
							1.5			-1.53726	-2.00633
							2			-1.42006	-2.00830
							2.5			-1.30397	-2.01065
							1.5	0.05		-1.53726	-2.00633

https://doi.org/10.71058/jodac.v10i01009

								0.1		-1.51699	-2.00664
								0.15		-1.49609	-2.00695
									0.05	-1.53726	-2.00633
									0.1	-1.52044	-2.00658
									0.15	-1.50359	-2.00683

Table 2: Numerical values of $Re_x^{-0.5}Nu_x$ and $Re_x^{-0.5}Sh_x$ for various physical parameters.

M	K	K_s	C_1	λ	α	R	θ_w	Ec_x	Ec_y	$Re_x^{-0.5}Nu_x$	$Re_x^{-0.5}Sh_x$
2	1	1	0.5	0.5	0.5	2	2	0.2	0.2	4.22270	-0.25238
0										5.70645	-0.30164
1										4.85840	-0.27550
2										4.22270	-0.25238
	0									4.22270	-0.32784
	0.5									4.22270	-0.29463
	1									4.22270	-0.25238
		0								4.22270	0
		1								4.22270	-0.25238
		1.5								4.22270	-0.27889
			0.5							4.22270	-0.25238
			1							4.33425	-0.38333
			2							-0.26448	-0.49573
				0.5						4.22270	-0.25238

https://doi.org/10.71058/jodac.v10i01009

				1						4.30899	-0.26466
				2						4.41251	-0.28395
					0.5					4.22270	-0.25238
					1					4.24584	-0.25541
					2					4.28724	-0.26107
						0				1.23148	-0.24029
						1				3.18702	-0.24698
						2				4.22270	-0.25238
							1.5			3.17132	-0.24723
							2			4.22270	-0.25238
							2.5			5.32674	-0.25861
							1.5	0.05		3.17132	-0.24723
								0.1		2.72258	-0.24802
								0.15		2.26707	-0.24884
									0.05	3.17132	-0.24723
									0.1	2.75866	-0.24787
									0.15	2.34552	-0.24850

https://doi.org/10.71058/jodac.v10i01009

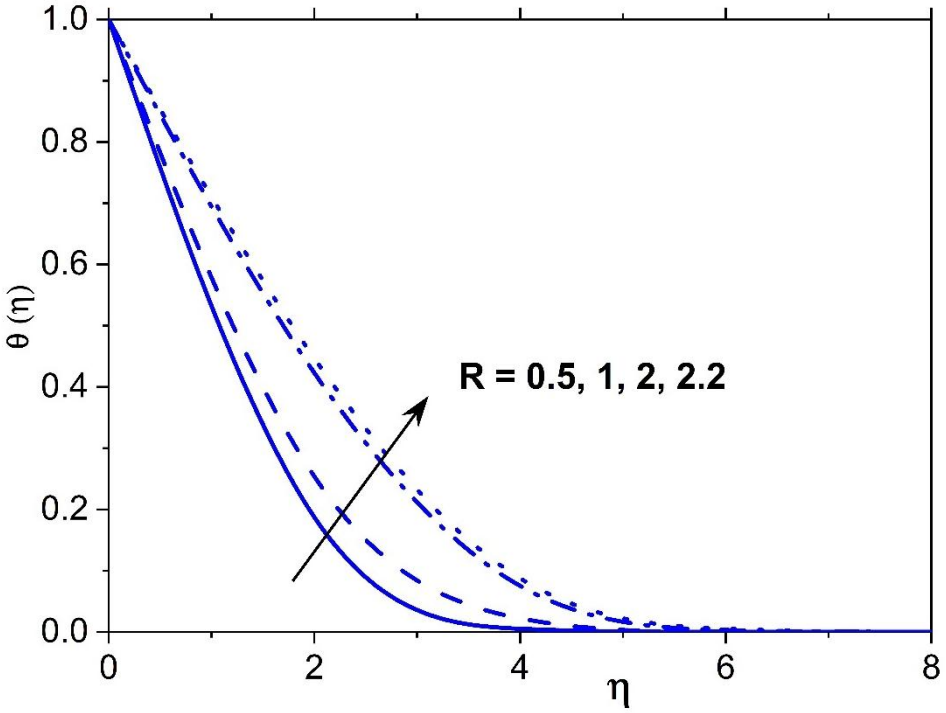

Fig:2. Influence of R on the temprature profile $\theta(\eta)$.

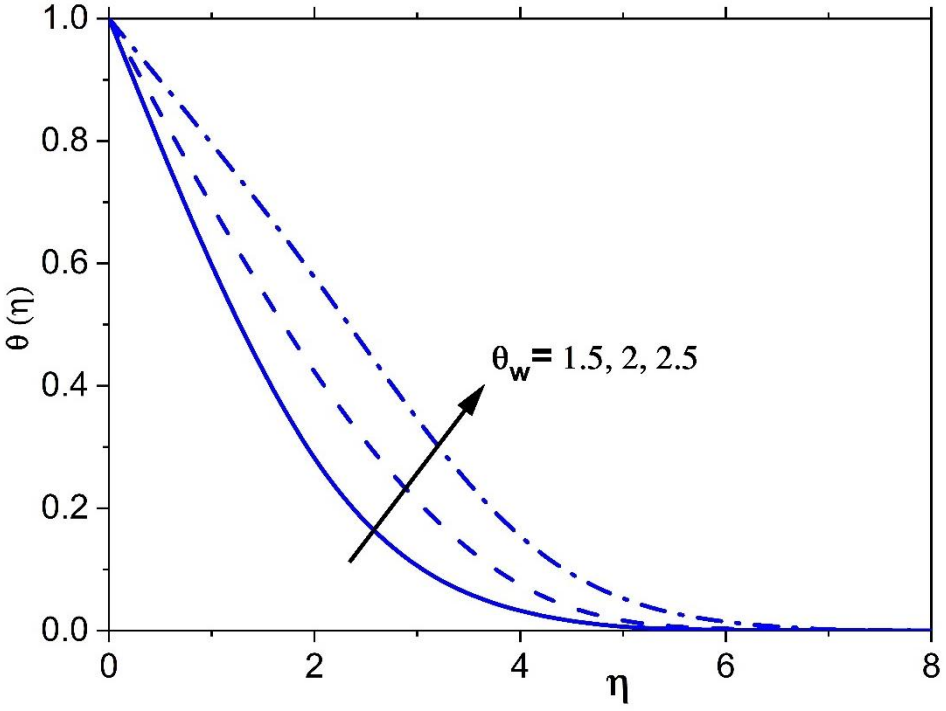

Fig:3. Influence of θ_w on the temprature profile $\theta(\eta)$.

https://doi.org/10.71058/jodac.v10i01009

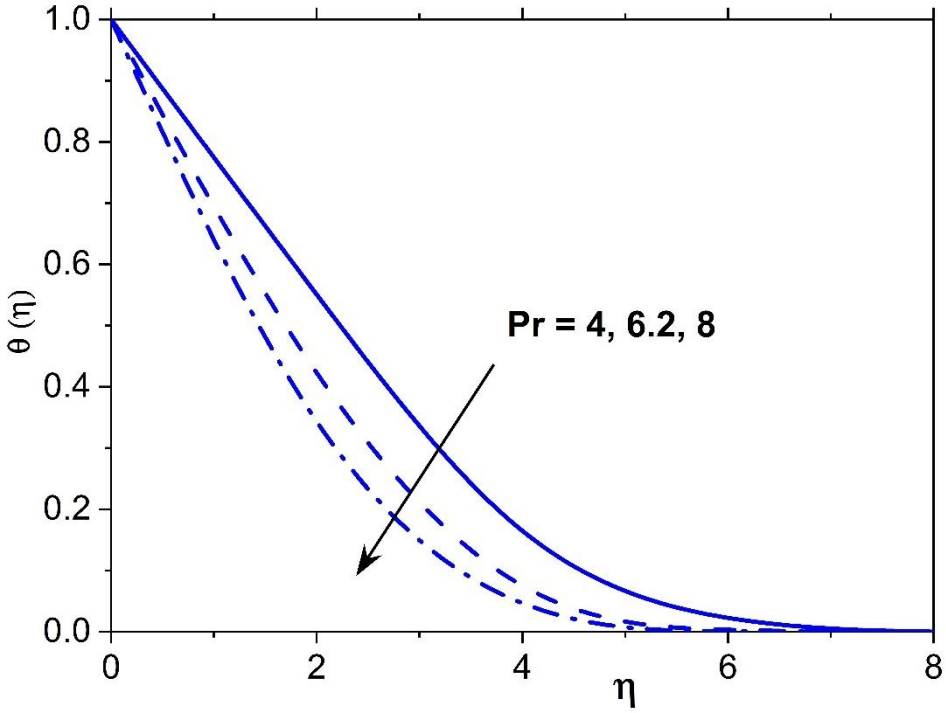

Fig:4. Influence of Pr on the temprature profile $\theta(\eta)$.

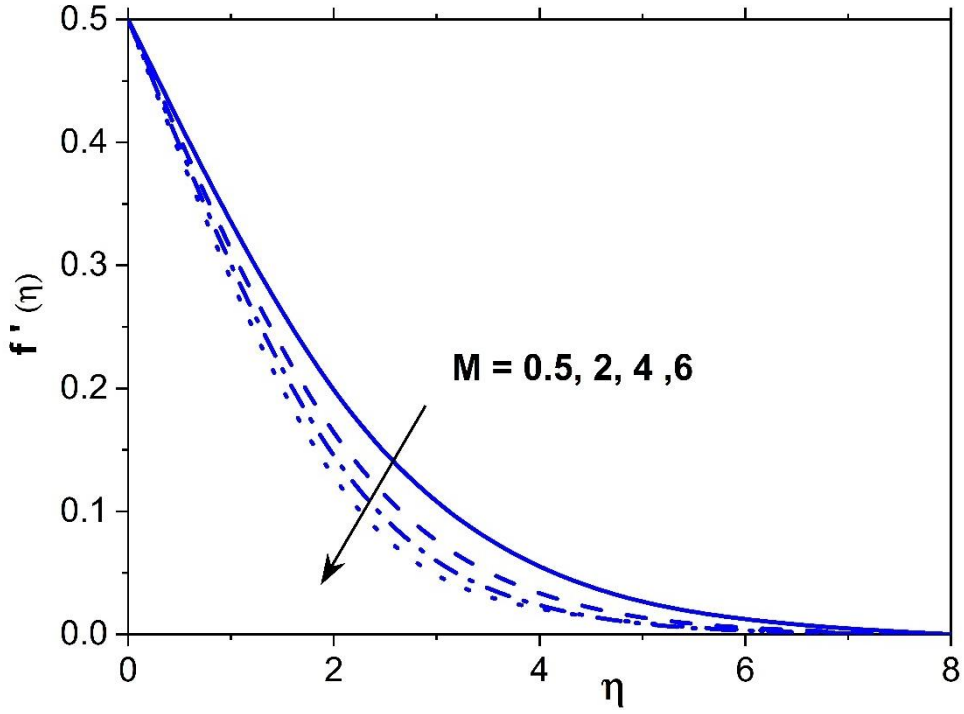

Fig:5. Influence of M on the velocity profile $f'(\eta)$.

https://doi.org/10.71058/jodac.v10i01009

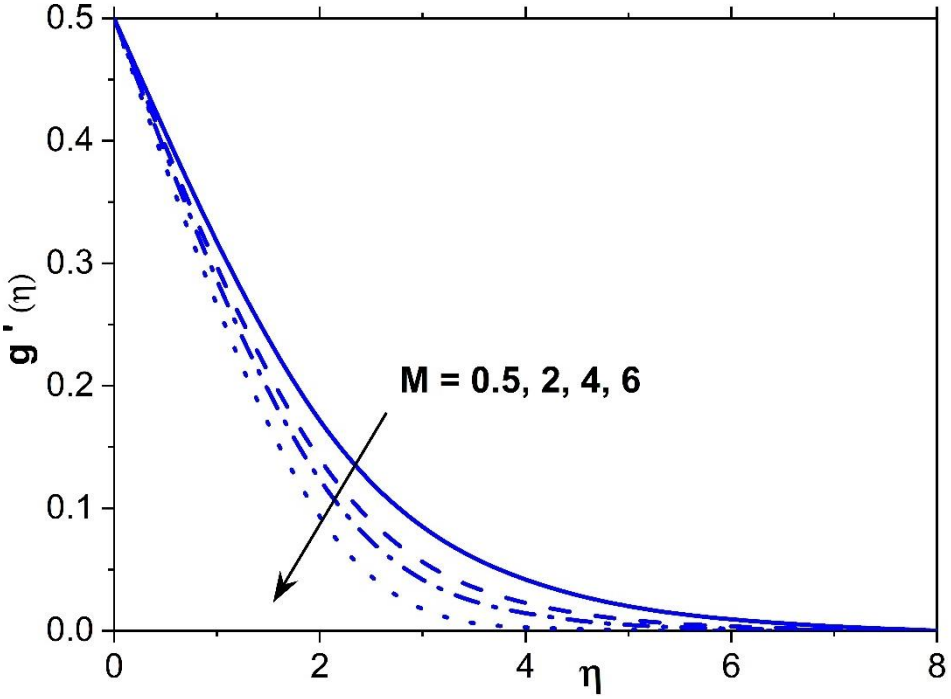

Fig:6. Influence of M on the velocity profile $g'(\eta)$.

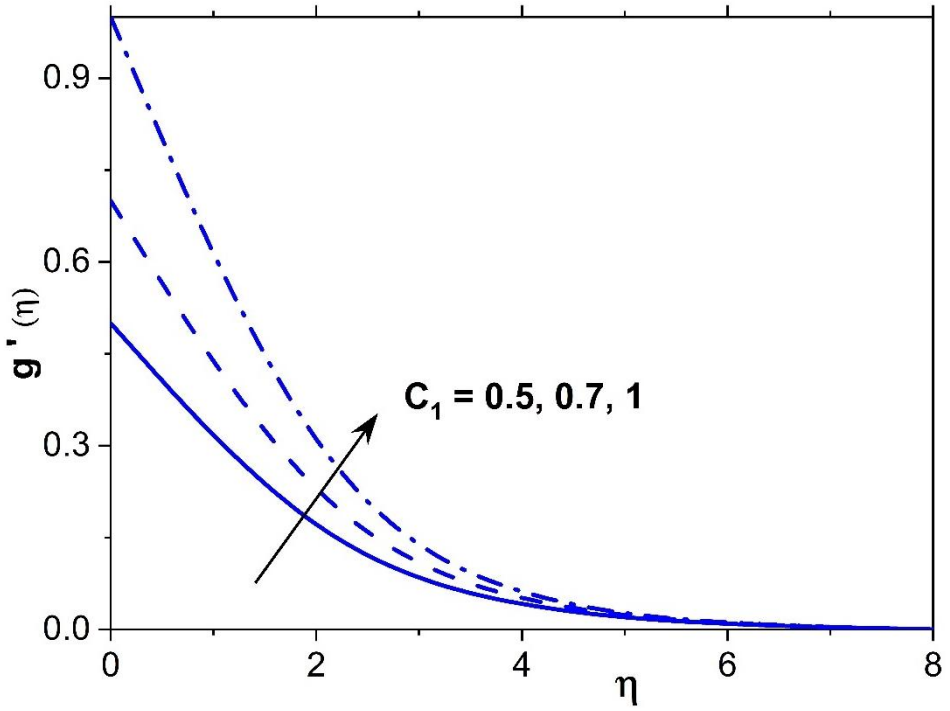

Fig:7. Influence of C_1 on the velocity profile $g'(\eta)$.

https://doi.org/10.71058/jodac.v10i01009

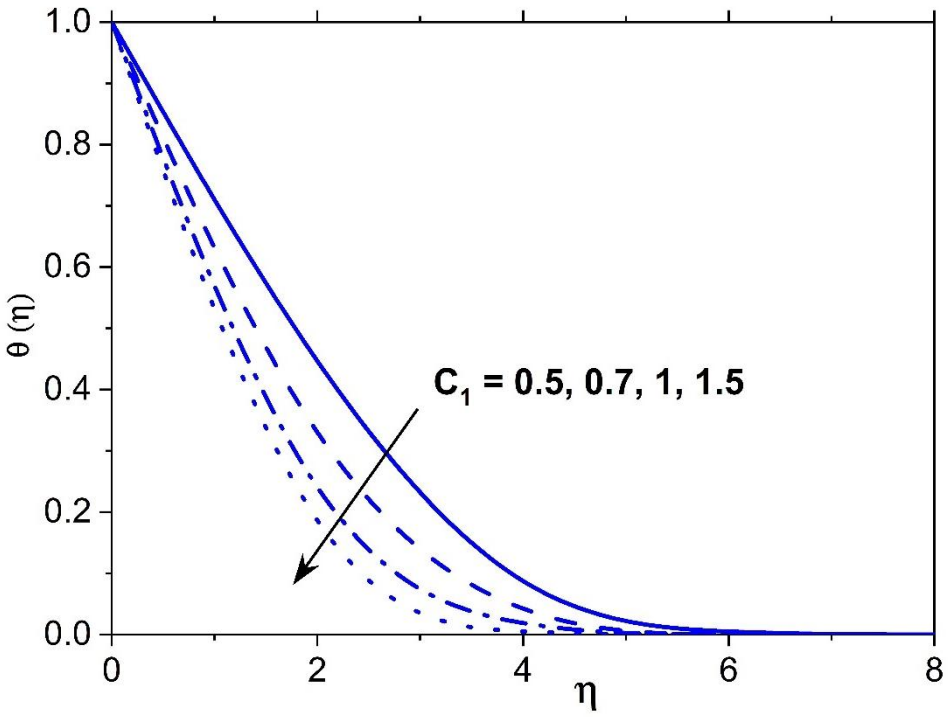

Fig:8. Influence of C_1 on the temparture profile $\theta(\eta)$.

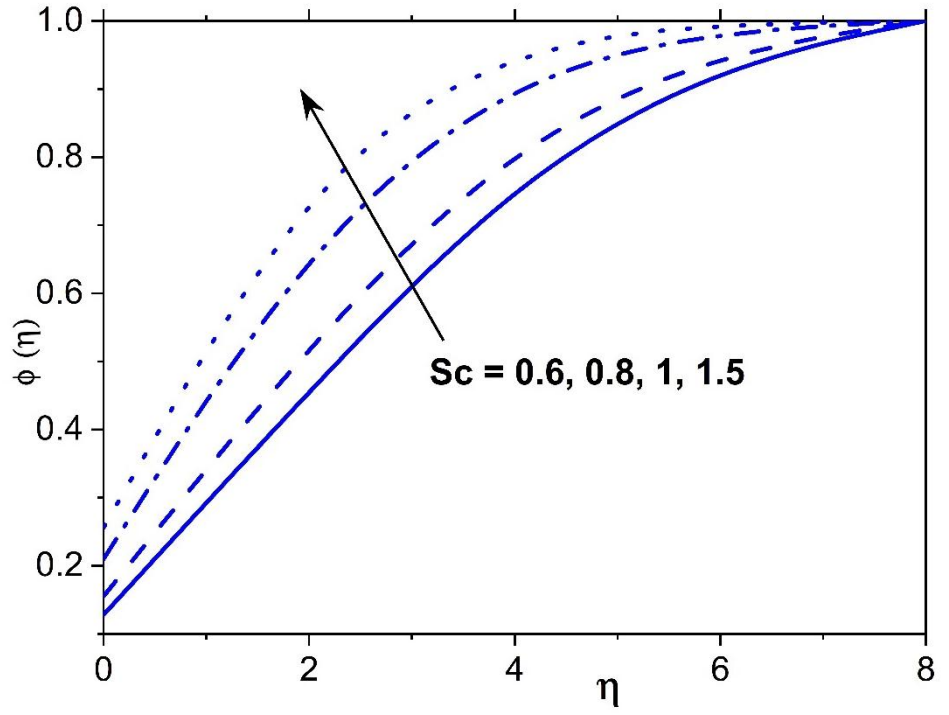

Fig:9. Influence of Sc on concentration profile $\phi(\eta)$.

https://doi.org/10.71058/jodac.v10i01009

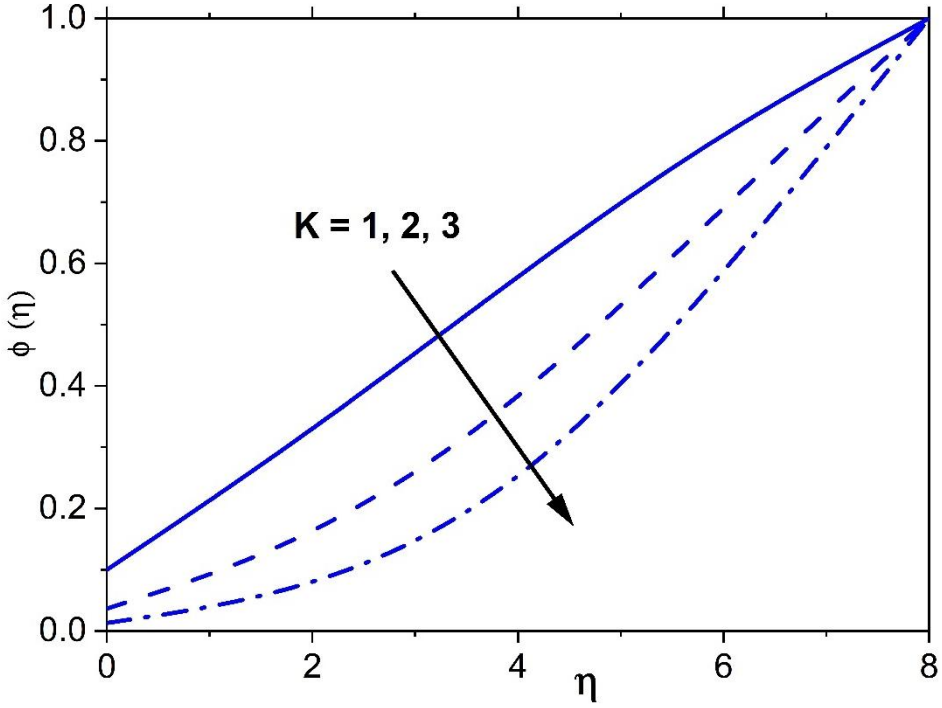

Fig:10. Influence of K on concentration profile $\phi(\eta)$.

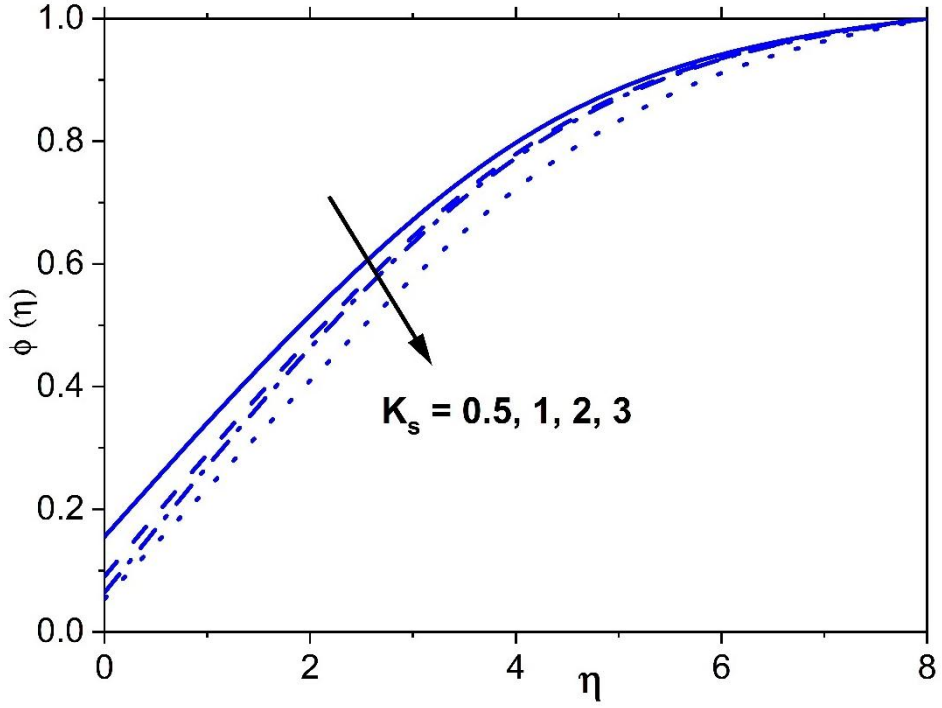

Fig:11. Influence of K_S on concentration profile $\phi(\eta)$.

https://doi.org/10.71058/jodac.v10i01009

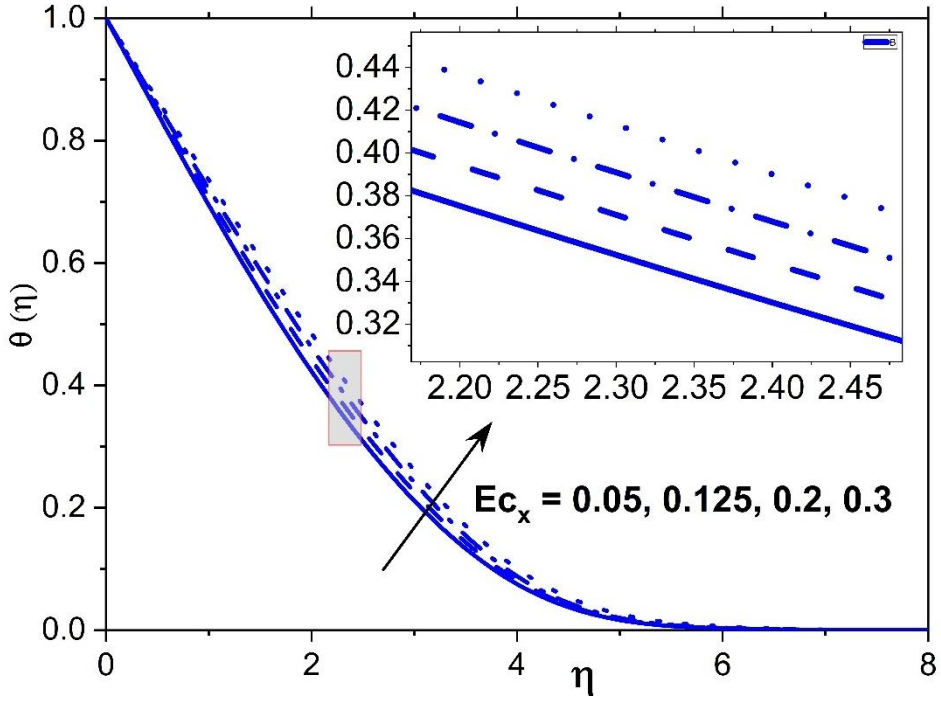

Fig:12. Influence of Ec_x on temparature profile $\theta(\eta)$.

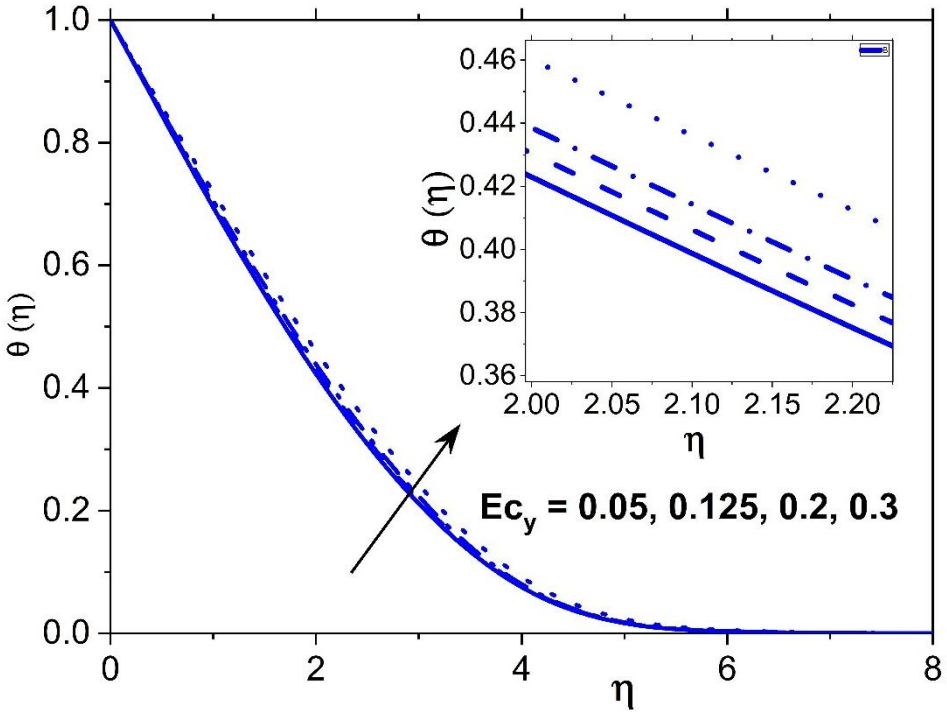

Fig:13. Influence of Ec_y on temparature profile $\theta(\eta)$.

https://doi.org/10.71058/jodac.v10i01009

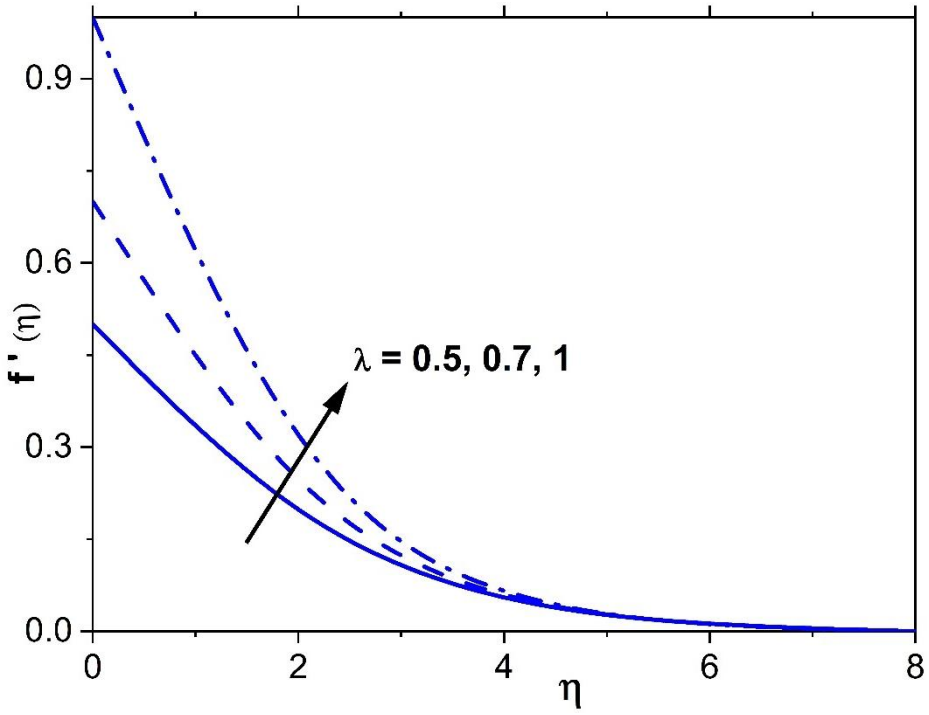

Fig:14. Influence of λ on velocity profile $f'(\eta)$.

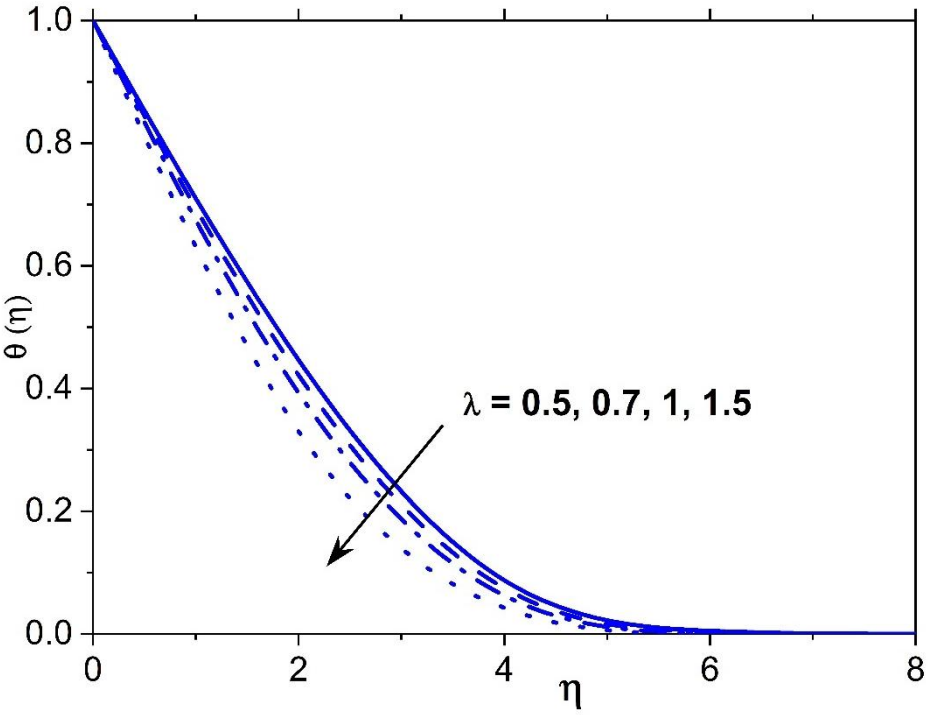

Fig:15. Influence of λ on temparature profile $\theta(\eta)$.

References

1. Casson, N. (1959). A flow equation for pigment-oil suspensions of the printing ink type. Rheology of Disperse Systems, 84–102.

https://doi.org/10.71058/jodac.v10i01009

2. Mustafa, M., Hayat, T., Pop, I., & Aziz, A. (2011). Stagnation-point flow and heat transfer of a Casson fluid. International Journal of Heat and Mass Transfer, 54(1–3), 558–563.
3. Nadeem, S., & Lee, C. (2012). MHD flow of a Casson fluid over a stretching sheet. Scientia Iranica, 19(6), 1550–1553.
4. Bhattacharyya, K. (2013). Slip effects on Casson fluid boundary layer over a stretching sheet. Ain Shams Engineering Journal, 4(3), 933–938.
5. Makanda, G., Sibanda, P., & Motsa, S. S. (2015). Chemical reaction and heat transfer in Casson fluid flow. Boundary Value Problems, 2015(1), 1–16.
6. Hayat, T., Javed, T., & Abbas, Z. (2009). Thermal radiation effects on Casson fluid flow. Nonlinear Analysis: Real World Applications, 10(5), 2010–2019.
7. Khan, W. A., & Pop, I. (2010). Boundary-layer flow of nanofluids past a stretching sheet. International Journal of Heat and Mass Transfer, 53, 2477–2483.
8. Nadeem, S., Haq, R. U., & Lee, C. (2014). Heat transfer analysis of Casson nanofluid over a stretching cylinder. Journal of Nanomaterials, 2014, 1–7.
9. Chambré, P. L., & Acrivos, A. (1956). On chemical surface reactions in laminar boundary layer flows. Journal of Applied Physics, 27(11), 1322-1328.
10. Chaudhary, M. A., & Merkin, J. H. (1995). A simple isothermal model for homogeneous-heterogeneous reactions in boundary-layer flow. I Equal diffusivities. Fluid dynamics research, 16(6), 311-333.
11. Chaudhary, M. A., & Merkin, J. H. (1995). A simple isothermal model for homogeneous-heterogeneous reactions in boundary-layer flow. II Different diffusivities for reactant and auto catalyst. Fluid dynamics research, 16(6), 335.
12. Khan, W. A., & Pop, I. (2010). Flow near the two-dimensional stagnation-point on an infinite permeable wall with a homogeneous–heterogeneous reaction. Communications in Nonlinear Science and Numerical Simulation, 15(11), 3435-3443.
13. Kameswaran, P. K., Shaw, S., Sibanda, P. V. S. N., & Murthy, P. V. S. N. (2013). Homogeneous–heterogeneous reactions in a nanofluid flow due to a porous stretching sheet. International journal of heat and mass transfer, 57(2), 465-472.
14. Hayat, T., Hussain, Z., Farooq, M., & Alsaedi, A. (2016). Effects of homogeneous and heterogeneous reactions and melting heat in the viscoelastic fluid flow. Journal of Molecular Liquids, 215, 749-755.

https://doi.org/10.71058/jodac.v10i01009

15. Xu, N. L., Xu, H., & Raees, A. (2018). Homogeneous-heterogeneous reactions in flow of nanofluids near the stagnation region of a plane surface: The Buongiorno's model. International Journal of Heat and Mass Transfer, 125, 604-609.
16. Nisar, K. S., Anjum, M. W., Raja, M. A. Z., & Shoaib, M. (2024). Homogeneous-heterogeneous reactions on Darcy-Forchheimer nanofluid flow system. Case Studies in Thermal Engineering, 53, 103882.
17. Ramya, N., Deivanayaki, M., Kavya, P., Loganathan, K., & Eswaramoorthi, S. (2025). Influence of homogeneous–heterogeneous reactions on micropolar nanofluid flow over an exponentially stretching surface with the Cattaneo–Christov heat flux model. *Discover Applied Sciences*, *7*(6), 554.
18. Reddy Gorla, Rama Subba, and Ibrahim Sidawi. "Free convection on a vertical stretching surface with suction and blowing." *Applied Scientific Research* 52, no. 3 (1994): 247-257.
19. T.Y. Wang, Mixed convection heat transfer from a vertical plate to non-Newtonian fluids" International Journal of Heat and Fluid Flow, 16 (1995) 56– 61.
20. A.J. Chamkha, Hydromagnetic three-dimensional free convection on a vertical stretching surface with heat generation or absorption, International Journal of Heat and Fluid Flow, 20 (1999) 84-92.
21. Rashidi, Mohammad Mehdi, Muhammad Ashraf, Behnam Rostami, Taher Mohammad Rastegari, and Sumra Bashir. "Mixed convection boundary-layer flow of a micro polar fluid towards a heated shrinking sheet by homotopy analysis method." *Thermal science* 20, no. 1 (2016): 21-34.
22. Gireesha, B. J., B. Mahanthesh, Rama Subba Reddy Gorla, and K. L. Krupalakshmi. "Mixed convection two-phase flow of Maxwell fluid under the influence of non-linear thermal radiation, non-uniform heat source/sink and fluid-particle suspension." *Ain Shams Engineering Journal* 9, no. 4 (2018): 735-746.
23. F.M. Ali, R. Nazar, N.M. Arifin, I. Pop, Mixed convection stagnation-point flow on vertical stretching sheet with external magnetic field, Applied Mathematics and Mechanics, 35(2) (2014) 155-166.
24. M.Y. Malik, I. Khan, A. Hussain, T. Salahuddin, Mixed convection flow of MHD Eyring-Powell nanofluid over a stretching sheet: A numerical study, AIP Advances, 5 (2015) 117-118.

https://doi.org/10.71058/jodac.v10i01009

25. B. Mahanthesh, B.J. Gireesha and R.S.R. Gorla, Heat and mass transfer effects on the mixed convective flow of chemically reacting nanofluid past a moving/stationary vertical plate, Alexandria Engineering Journal, 55(1) (2016) 569–581.
26. S. Das, R.N. Jana, O.D. Makinde, Mixed convective magnetohydrodynamic flow in a vertical channel filled with nanofluids, Engineering Science and Technology, an International Journal, 18(2) (2015) 244-255.
27. K. Vajravelu, J.R. Cannon, J. Leto, R. Semmoum, N. Nathan, M. Draper, D. Hammock, Nonlinear convection at a porous flat plate with application to heat transfer from a dike, Journal of mathematical analysis and applications, 277 (2003) 609-623.
28. P.K. Kameswaran, P. Sibanda, M.K. Partha, P.V.S.N. Murthy, Thermophoretic and non-linear convection in non-Darcy porous medium, Journal of Heat Transfer, ASME, 136(4) (2014) 042601.
29. S. Shaw, G. Mahanta, P. Sibanda, Non-linear thermal convection in a Casson fluid flow over a horizontal plate with convective boundary condition, Alexandria Engineering Journal, 55(2) (2016) 1295–1304.
30. Jyoti, D. K., V. Nagaradhika, P. B. Sampath Kumar, and Ali J. Chamkha. "Nonlinear Convection and Radiative Heat Transfer in Kerosene-Alumina Nanofluid Flow Between Two Parallel Plates with Variable Viscosity." *Journal of Nanofluids* 13, no. 5 (2024): 1055-1062.
31. Shoaib, Muhammad, Shafaq Naz, Muhammad Asif Zahoor Raja, Khadeeja Arshad, Iftikhar Ahmad, and Kottakkaran Sooppy Nisar. "Numerical treatment for nonlinear mixed convection and thermal radiative Newtonian fluid flow system." *Journal of Radiation Research and Applied Sciences* 18, no. 3 (2025): 101675.